Accurate Differentiation of Recurrent Gliomas from Radiation Injury by Kinetic Analysis of α-11C-Methyl-L-Tryptophan PET

Bálint Alkonyi[1], Geoffrey R. Barger[2,3], Sandeep Mittal[3,4], Otto Muzik[1,5,6], Diane C. Chugani[1,5], Gautam Bahl[6], Natasha L. Robinette[3,6], William J. Kupsky[7], Pulak K. Chakraborty[1,6], and Csaba Juhász[1,2,3,5]

[1]PET Center, Children's Hospital of Michigan, Detroit, Michigan; [2]Department of Neurology, Wayne State University School of Medicine, Detroit, Michigan; [3]Karmanos Cancer Institute, Detroit, Michigan; [4]Department of Neurosurgery, Wayne State University, Detroit, Michigan; [5]Department of Pediatrics, Wayne State University, Detroit, Michigan; [6]Department of Radiology, Wayne State University, Detroit, Michigan; and [7]Department of Pathology, Wayne State University, Detroit, Michigan

PET of amino acid transport and metabolism may be more accurate than conventional neuroimaging in differentiating recurrent gliomas from radiation-induced tissue changes. α-11C-methyl-L-tryptophan (11C-AMT) is an amino acid PET tracer that is not incorporated into proteins but accumulates in gliomas, mainly because of tumoral transport and metabolism via the immunomodulatory kynurenine pathway. The aim of this study was to evaluate the usefulness of 11C-AMT PET supplemented by tracer kinetic analysis for distinguishing recurrent gliomas from radiation injury. **Methods:** Twenty-two 11C-AMT PET scans were obtained in adult patients who presented with a lesion suggestive of tumor recurrence on conventional MRI 1–6 y (mean, 3 y) after resection and postsurgical radiation of a World Health Organization grade II–IV glioma. Lesional standardized uptake values were calculated, as well as lesion-to-contralateral cortex ratios and 2 kinetic 11C-AMT PET parameters (volume of distribution [VD], characterizing tracer transport, and unidirectional uptake rate [K]). Tumor was differentiated from radiation-injured tissue by histopathology ($n = 13$) or 1-y clinical and MRI follow-up ($n = 9$). Accuracy of tumor detection by PET variables was assessed by receiver-operating-characteristic analysis. **Results:** All 11C-AMT PET parameters were higher in tumors ($n = 12$) than in radiation injury ($n = 10$) ($P \leq 0.012$ in all comparisons). The lesion-to-cortex K-ratio most accurately identified tumor recurrence, with highly significant differences both in the whole group ($P < 0.0001$) and in lesions with histologic verification ($P = 0.006$); the area under the receiver-operating-characteristic curve was 0.99. A lesion-to-cortex K-ratio threshold of 1.39 (i.e., a 39% increase) correctly differentiated tumors from radiation injury in all but 1 case (100% sensitivity and 91% specificity). In tumors that were high-grade initially ($n = 15$), a higher lesion-to-cortex K-ratio threshold completely separated recurrent tumors (all K-ratios ≥ 1.70) from radiation injury (all K-ratios < 1.50) (100% sensitivity and specificity). **Conclusion:** Kinetic analysis of dynamic 11C-AMT PET images may accurately differentiate between recurrent World Health Organization grade II–IV infiltrating gliomas and radiation injury. Separation of unidirectional uptake rates from transport can enhance the differentiating accuracy of 11C-AMT PET. Applying the same approach to other amino acid PET tracers might also improve their ability to differentiate recurrent gliomas from radiation injury.

Key Words: glioma; tumor recurrence; radiation injury; positron emission tomography; tryptophan; kinetic analysis

Initial treatment of low-grade and high-grade gliomas includes surgery, radiation therapy, or chemotherapy. After initial treatment, gliomas often recur. Diagnosing recurrent tumor after radiation is complicated by the common occurrence of radiation injury, frequently referred to as radiation necrosis. Optimal choice of therapy should rely on an accurate distinction between radiation injury and true tumor recurrence, but currently there is no widely accepted noninvasive diagnostic test capable of discriminating between these 2 entities. Both radiation injury and tumor recurrence commonly manifest as a new, often progressive contrast-enhancing lesion or a T2 or fluid-attenuated inversion recovery abnormality on conventional MRI (1,2), typically within or near the surgical resection bed. The similar clinical presentation and radiologic appearance make accurate differentiation between radiation-related lesions, which may occur up to 10 y after irradiation, and true tumor recurrence challenging (1–3).

Several advanced imaging modalities (including perfusion MRI, proton MR spectroscopy (1H-MRS), and PET using amino acid radiotracers) have shown promise in the differentiation of brain tumor recurrence from treatment effects (4). Among PET techniques, imaging with 11C-labeled methionine and O-(2-18F-fluoroethyl)-L-tyrosine (18F-FET) have been studied extensively (5–9). Posttreatment 11C-methionine PET studies typically measured standardized uptake values (SUVs) in lesions and contralateral cortex (5,8,9). In

one of the largest ^{11}C-methionine PET studies (8) (including 26 gliomas and 51 metastatic brain tumors), both sensitivity and specificity in separating recurrent tumors from radiation injury varied between 75% and 79%. ^{18}F-FET PET measures transport of tumoral amino acid, because it is not incorporated into proteins or metabolized. ^{18}F-FET PET studies, also using SUVs, showed sensitivity and specificity up to 100% for identifying recurrent gliomas (6,7,9). In 1 study, analysis of dynamic ^{18}F-FET SUV changes also demonstrated a high accuracy in differentiating low-grade from high-grade gliomas after treatment (10).

α-^{11}C-methyl-L-tryptophan (^{11}C-AMT) is an amino acid PET tracer that can measure tryptophan metabolism via the immunomodulatory kynurenine pathway (11–13). We have shown that ^{11}C-AMT accumulates because of both transport and metabolism in both untreated and recurrent World Health Organization (WHO) grade II–IV gliomas (14–16). Whether ^{11}C-AMT would be useful in differentiating between recurrent gliomas and radiation-induced injury was unknown. Our previous studies demonstrated that tumoral transport of ^{11}C-AMT is affected by a defective blood–brain barrier (as indicated by gadolinium enhancement on MRI) (14), which is common in both high-grade gliomas and radiation-injured tissue. Therefore, we believed that ^{11}C-AMT metabolic rates might be more accurate than transport rates in differentiating radiation injury from true tumor recurrence. In the present study, we performed kinetic analysis of dynamic brain PET scans combined with blood radioactivity data, which allows separation of ^{11}C-AMT transport and metabolic rates, to determine whether ^{11}C-AMT PET could reliably differentiate recurrent gliomas from radiation-induced changes in patients who present with conventional MRI abnormalities suggestive of recurrence of WHO grade II–IV gliomas. We aimed to determine which ^{11}C-AMT PET-derived kinetic parameter would provide the best accuracy for tumor detection and whether this parameter performs better than SUV.

MATERIALS AND METHODS

Patients

Twenty-one adults (age at ^{11}C-AMT PET scan, 30–68 y; Table 1) with a history of resection of a WHO grade II–IV glioma underwent ^{11}C-AMT PET using a research protocol. One patient (patient 2 in Table 1) underwent ^{11}C-AMT PET twice, at a 1-y interval, with each scan followed by resection of the suggestive lesion; both of his ^{11}C-AMT PET scans were analyzed. All patients had undergone radio- or chemoradiotherapy after initial surgery and showed potential tumor recurrence or radiation injury because of an enlarging contrast-enhancing or hyperintense T2 or fluid-attenuated inversion recovery lesion on MRI. All had at least 1 y of follow-up or subsequent histology (from the resected lesion) for the diagnosis of tumor recurrence or radiation injury. The original tumors were WHO grade II in 7 patients, grade III in 5, and grade IV (glioblastoma) in 9. Conventional fractionated external-beam partial-brain radiotherapy over 6 wk, with a total radiation dose typically between 54 and 60 Gy, was started within 4 wk after initial surgery. Most patients also underwent adjuvant chemotherapy with temozolomide. The mean interval between initial surgical resection and ^{11}C-AMT PET was 3.1 y

(range, 1–6.3 y). In addition, clinical ^{18}F-FDG PET was also performed in 9 patients within 1 d to 10 mo (median, 14 d) of the ^{11}C-AMT PET. The study was approved by the Wayne State University Institutional Review Board, and written informed consent was obtained from all participants.

Tumor recurrence versus radiation injury without active tumor was determined as follows: lesions were defined as tumor recurrence if subsequent histopathologic examination of resected suggestive lesions showed evidence of tumor at the same or higher grade, or if there was clinical deterioration plus growth of a contrast-enhancing lesion on serial MRI during a 1-y follow-up after the ^{11}C-AMT PET scan. These MRI studies were performed within 1 mo of the ^{11}C-AMT PET and then at 2- to 6-mo intervals thereafter. All patients whose serial MRI studies were used to determine presence or absence of tumor underwent at least 3 MRI scans after the ^{11}C-AMT PET. Lesions were defined as radiation injury with no tumor recurrence if subsequent histopathology verified the presence of radiation injury without evidence of definite tumor, or if the patient remained clinically stable or improved, with a stable or diminishing contrast-enhancing or hyperintense T2 or fluid-attenuated inversion recovery lesion on serial MRI during a 1-y follow-up after the ^{11}C-AMT PET scan.

Differentiation Between Tumor and Radiation Injury on Histopathology

Routine neuropathologic examination after formalin fixation and embedding in paraffin was performed by a neuropathologist. Hematoxylin and eosin staining was supplemented by special stains, including immunohistochemical staining for glial fibrillary acidic protein to assess cell morphology, Ki-67 to assess proliferative activity, CD34 (or Masson trichrome stain) to assess vascular structure and density, and CD68 to assess for the presence of macrophages and microglial activation. The presence of tumor was determined by findings of infiltrative or solid tumor showing pleomorphic glial cells with nuclear atypia, areas of high cell density, and presence of mitotic activity or Ki-67 immunoreactivity in the tumor cell population. Microvascular proliferation and focal necrosis with pseudopalisading, when present, were considered characteristics of recurrent tumor. The presence of radiation injury was determined by findings of areas of coagulative necrosis in brain tissue, sclerotic or ectatic blood vessels, fibrinoid necrosis in blood vessels, and nuclear atypia in mural cells in blood vessel walls. Patients with any evidence of definite tumor during histologic examination were classified as having tumor recurrence. Patients with radiation injury and only isolated atypical glial cells scattered in hypocellular brain tissue were classified as no tumor recurrence.

PET Protocols

All ^{11}C-AMT PET studies were performed using the EXACT/ HR whole-body positron tomograph (CTI/Siemens) located at the Children's Hospital of Michigan in Detroit. This scanner has a 15-cm field of view and generates 47 image planes with a slice thickness of 3.125 mm. The reconstructed image resolution obtained is 7.5 ± 0.4 mm in full width at half maximum in-plane and 7.0 ± 0.5 mm in the axial direction. The procedure for ^{11}C-AMT PET has been described previously (13,14). In brief, after the patient had fasted for 6 h, a venous line was established for injection of ^{11}C-AMT (3.7 MBq/kg) as a slow bolus over 2 min. A second venous line was established for collection of timed blood samples (0.5 mL/sample, collected at 20, 30, 40, 50, and 60 min after ^{11}C-AMT injection). Initially, coinciding with tracer injection, a 20-min

TABLE 1
Clinical and Quantitative ^{11}C-AMT PET Data of Patients

No.	Age (y)	Sex	Tumor type	WHO grade	Postsurgical treatment	Histology	Recurrence	Time since surgery (y)	SUV	SUV ratio	K (mL/g/min)	K ratio	VD	VD ratio
1	31	M	Oligo	2(3)	Rad + chemo	Yes	Yes	1.5	2.18	1.35	0.007	1.60*	0.47	1.30
2a	31	M	Astro	2(3)	Rad + chemo	Yes	Yes	2	1.84	1.91	0.009	1.71	0.55	2.75
3	34	F	AO	3(3)	Rad	Yes	Yes	4	3.75	2.98	0.022	2.75	1.06	3.53
4	36	M	GBM	4(4)	Rad + chemo	Yes	Yes	3	2.37	1.60	0.008	2.40	0.42	1.50
5	45	M	AO	3(3)	Rad + chemo	Yes	Yes	2.8	3.82	3.23	0.019	3.30	1.75	5.00
6	47	M	Oligo	2(3)	Rad	Yes	Yes	4.2	1.45	2.55	0.013	2.60	0.57	2.85
7	47	M	AO	3(4)	Rad	Yes	Yes	2.2	1.87	1.67	0.009	1.70	0.56	2.70
8	56	M	GBM	4(4)	Rad + chemo	Yes	Yes	2.5	2.20	2.64	0.013	2.10	1.16	5.20
9	58	M	OA	2	Rad	No	Yes	1	2.12	1.32	0.005	1.40	0.40	1.60
10	59	F	Oligo	2(3)	Rad	Yes	Yes	6	5.11	2.94	0.011	2.40†	0.85	4.20
11	61	M	GBM	4	Rad + chemo	No	Yes	1	2.59	1.77	0.013	2.00	0.97	6.30
12	68	M	GBM	4	Rad	No	Yes	1.3	2.84	1.78	0.014	2.00	0.67	3.00
13	30	M	AOA	3	Rad + chemo	No	No	5	1.78	0.91	0.005	0.94	0.38	1.03
2b	32	M	AA	3	Rad + chemo	Yes	No	3	1.65	1.43	0.007	1.18	0.55	2.00
14	41	F	GBM	4	Rad + chemo	Yes	No	5	1.82	1.54	0.010	1.49	0.52	2.50
15	41	F	GBM	4	Rad + chemo	Yes	No	3.1	2.59	1.41	0.007	1.20	0.81	2.45
16	43	M	OA	2	Rad + chemo	No	No	2.2	1.16	1.02	0.004	0.89	0.23	1.10
17	48	M	AA	3	Rad + chemo	No	No	5	1.33	0.99	0.004	1.15	0.30	0.97
18	53	F	Oligo	2	Rad	No	No	6.3	0.95	0.81	0.003	1.05	0.18	0.66
19	58	F	GBM	4	Rad	No	No	2.2	1.94	1.32	0.006	1.20	0.45	1.76
20	60	M	GBM	4	Rad + chemo	Yes	No	1.8	1.84	1.45	0.008	1.30	0.36	2.15
21	63	M	GBM	4	Rad	No	No	4	2.06	1.27	0.007	1.37	0.33	1.43

*A second lesion (also histologically verified recurrent tumor) had K ratio of 1.51.

†A second lesion (also histologically verified recurrent tumor) had K ratio of 1.80.

Oligo = oligodendroglioma; astro = astrocytoma; AO = anaplastic oligodendroglioma; GBM = glioblastoma; OA = oligoastrocytoma; AOA = anaplastic oligoastrocytoma; AA = anaplastic astrocytoma; rad = radiation therapy; chemo = chemotherapy.

Ratios indicate lesion-to-contralateral cortex ratios. Histology refers to histologic verification of recurrent tumor vs. radiation injury. WHO grades in parenthesis indicate tumor grade determined by histologic assessment of recurrent glioma. Patient 2 had two ^{11}C-AMT PET scans (2a and 2b), each followed by surgical resection and histopathologic examination (which showed tumor first but radiation injury the second time).

dynamic PET scan of the heart was performed (twelve 10-s scans, three 60-s scans, and three 300-s scans) in 2-dimensional mode to obtain the blood input function from the left ventricle of the heart. The blood input function was continued beyond this initial 20 min by using venous blood samples as described previously (17). At 25 min after tracer injection, a dynamic emission scan of the brain (7 × 5 min) was acquired in high-sensitivity 3-dimensional mode. Measured attenuation correction using a rotating ^{68}Ge rod source was applied to the ^{11}C-AMT PET images of the heart, whereas computed attenuation correction was used to correct the brain images.

Clinical ^{18}F-FDG PET scans were obtained in 9 patients. These scans were performed either using the EXACT/HR PET scanner or using a Discovery STE PET/CT scanner (GE Healthcare). The reconstructed in-plane and axial resolutions for the EXACT/HR scanner are 5.0 ± 0.2 mm and 5.8 ± 0.4 mm, respectively, in full width at half maximum. The Discovery PET/CT scanner has an isotropic image resolution of 6.0 ± 0.5 mm in full width at half maximum. ^{18}F-FDG (5.3 MBq/kg) was injected intravenously. Attenuation on the PET/CT scanner was corrected using a low-level CT scan (100 keV, 80 mA); all other scanning parameters were similar to those used for the EXACT/HR PET scanner.

^{11}C-AMT PET Image Analysis

Quantification of ^{11}C-AMT transport and metabolism was performed with the Patlak graphical approach (18) using the blood input function (combination of the radioactivity measured in the center of the left ventricle of the heart and from the venous blood samples) and the dynamic brain sequence, as described previously (14,15). This approach provides 2 kinetic parameters: the slope parameter, which reflects the unidirectional uptake of tracer into tissue (K), and the y-intercept of the Patlak plot representing the tracer's volume of distribution (VD), characterizing the net transport of tryptophan into the tissue. The advantages and limitations of using these parameters have been discussed previously (19,20). Blood metabolite analysis and correction were omitted, on the basis of the assumption that metabolites of ^{11}C-AMT constitute a small fraction of the activity in plasma (21,22).

Regions of interest (ROIs) were drawn on ^{11}C-AMT summed uptake images from 30 to 55 min after tracer injection. ROIs included areas suggestive of tumor recurrence on MRI and additional regions with apparently increased ^{11}C-AMT uptake, if present, as compared with the surrounding cortex. The software ROI Editor 1.4.1 (www.mristudio.org) was used, and ROIs were drawn in at least 3 adjacent axial PET image slices in each patient. To diminish partial-volume effects, the very edge (~1–2 mm from the edge) of regions with high uptake and regions with apparent central necrosis were excluded. ROI volumes ranged from 1.5 to 34.5 cm³. SUVs were obtained by dividing the average radioactivity concentration (kBq/cm³) of each region by the injected dose per total body weight (MBq/kg). The ROIs were applied to the

dynamic image sequence, and kinetic parameters were calculated from the time–activity curves using Patlak graphical analysis (*18*). In the 2 patients with 2 separate areas of increased ^{11}C-AMT uptake (Fig. 1), both areas were analyzed. To obtain lesion-to-cortex ratios, ROIs of similar size were drawn in the contralateral homotopic cortex (Fig. 1), and SUVs and kinetic parameters were obtained as described above.

Study Design and Statistical Analysis

Lesion-to-contralateral cortex ratios were calculated for SUV as well as for the kinetic parameters (K and VD), yielding SUV ratios, K ratios, and VD ratios for each patient. In the 2 patients with 2 separate areas of increased ^{11}C-AMT uptake, the region with the higher uptake was used for subsequent analysis. All kinetic values were compared between recurrent glioma and radiation injury in all patients and in the subgroup with histologic verification ($n = 13$), and, for exploratory purposes, we also analyzed a subgroup of patients with high-grade (grade III or IV) glioma at their original diagnosis ($n = 15$), using multivariate ANOVA. In addition, the receiver-operating-characteristic curve was analyzed to determine the most accurate ^{11}C-AMT PET–related variable and an optimal cutoff (with highest sensitivity plus specificity) for the differentiation of glioma recurrence from radiation-induced changes. Statistical analysis was performed using the software IBM SPSS Statistics, version 19.0 (SPSS Inc.). A *P* value of less than 0.05 was considered significant.

RESULTS

Clinical and quantitative imaging data of all patients are provided in Table 1. Tumor recurrence was determined in 12 patients (verified by histology in 9), and no evidence of tumor was found in 10 patients (verified by histology in 4; based on 1-y follow-up in 6). Patient 2 had histologically verified tumor recurrence after the first ^{11}C-AMT PET scan (2a in Table 1) and histologically verified radiation injury after reoperation after the second ^{11}C-AMT PET scan (2b in Table 1) 1 y later.

Visual assessment of the nine ^{18}F-FDG PET scans showed foci of increased metabolism near the resection bed in 4 patients with glioma recurrence and in 1 patient with radiation injury. Hypometabolic lesions, with ^{18}F-FDG uptake below normal cortical uptake, were seen in 3 patients with a recurrent glioma (all grade II on original histology [Fig. 1B]) and in 1

patient without tumor recurrence. Visual assessment of summed ^{11}C-AMT uptake (SUV) images showed increased ^{11}C-AMT uptake in the resection area in all 12 patients with glioma recurrence (see example in Fig. 1, where 2 separate areas showed ^{11}C-AMT increases) and in 4 of the 10 patients without recurrence. Figure 2 compares a case of recurrent glioma with a case of radiation injury. Although both lesions showed contrast enhancement and increased ^{11}C-AMT uptake on visual assessment (Figs. 2A–2D), kinetic analysis showed higher K (increased slope) and slightly increased VD in the tumor (Fig. 2E).

For all patients studied, every calculated ^{11}C-AMT PET parameter showed a significantly higher value in tumor than in radiation injury (Table 2). Among all the parameters, the lesion-to-cortex K-ratio differed the most significantly between these 2 groups (mean ± SD, 2.16 ± 0.55 vs. 1.18 ± 0.18; $P = 0.00003$). In the subgroup with histologic verification ($n = 13$), the difference between recurrent tumor and radiation injury remained highly significant for K-ratio ($P = 0.006$) and significant for SUV ratio ($P = 0.034$) but not for the other parameters (Table 2). In the subgroup of patients with high-grade tumor on original histology ($n = 15$), all PET parameters were again significantly different between recurrent tumor and radiation injury ($P \leq 0.014$ in all comparisons).

In the receiver-operating-characteristic analysis, the lesion-to-cortex K-ratio performed the best among all the ^{11}C-AMT PET parameters; the area under the curve (AUC) was 0.99. For all patients, a K-ratio threshold value of 1.39 (i.e., a 39% increase in the lesion) identified recurrent tumors with 100% sensitivity and 91% specificity. Using this cutoff threshold, only a single lesion (with a lesion-to-cortex K-ratio of 1.49) was falsely classified: this was a large contrast-enhancing lesion in a woman (patient 14 in Table 1) with a history of a heavily treated and reirradiated glioblastoma, whose complete resection of the suggestive lesion, 7 y after the original surgery, showed no evidence of recurrent tumor. Increasing the K-ratio threshold to 1.50 would have classified this lesion correctly but would have falsely classified another lesion (in patient 9) as a nontumorous lesion. In the receiver-operating-characteristic analysis, the AUC was
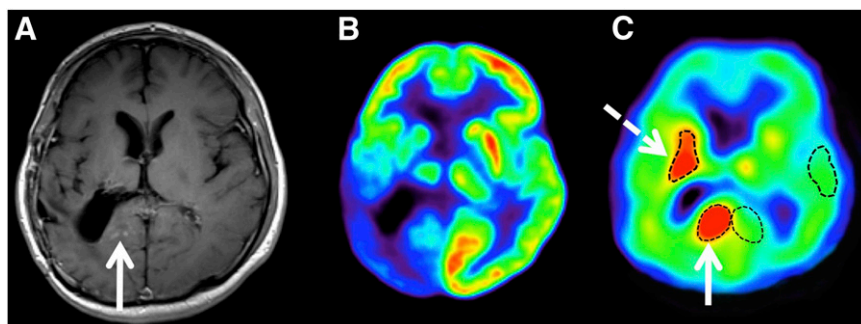

FIGURE 1. Coregistered T1-weighted postgadolinium MR (A), ^{18}F-FDG PET (B), and ^{11}C-AMT PET (C) images of 31-y-old man (patient 1) with surgically resected WHO grade II oligodendroglioma and suspected tumor recurrence. ^{18}F-FDG PET showed marked glucose hypometabolism in neighboring cortex, whereas ^{11}C-AMT PET demonstrated increased tryptophan uptake in area with mild contrast enhancement (solid arrows) and in more anterior region without contrast enhancement (dashed arrow). K and K lesion-to-cortex ratios of these 2 areas were similar (posterior area: 0.0070 mL/g/min and 1.60, respectively; anterior area: 0.0066 mL/g/min and 1.51, respectively). Repeated surgery demonstrated grade III oligodendroglioma in both areas.

FIGURE 2. Representative T1-weighted postgadolinium MR and coregistered ^{11}C-AMT PET images of patient with histologically verified glioma recurrence (A and C; patient 6) and patient with pure radiation injury, also verified by histology (B and D; patient 20). MR images showed contrast enhancement in both patients: small contrast-enhancing nodule medial to resection cavity in patient 6 (white arrow; A) and extensive contrast enhancement surrounding resection cavity in patient 20 (B). ^{11}C-AMT PET summed images from 30 to 60 min after tracer injection demonstrated markedly increased uptake of ^{11}C-AMT in both patients. However, kinetic analysis of dynamic PET images (E) revealed higher K (increased slope) and VD (higher y intercept) in recurrent glioma than in area of radiation injury. x-axis represents transformed time (blood time) in minutes. C_t = tracer concentration in tissue; C_p = tracer concentration in plasma.
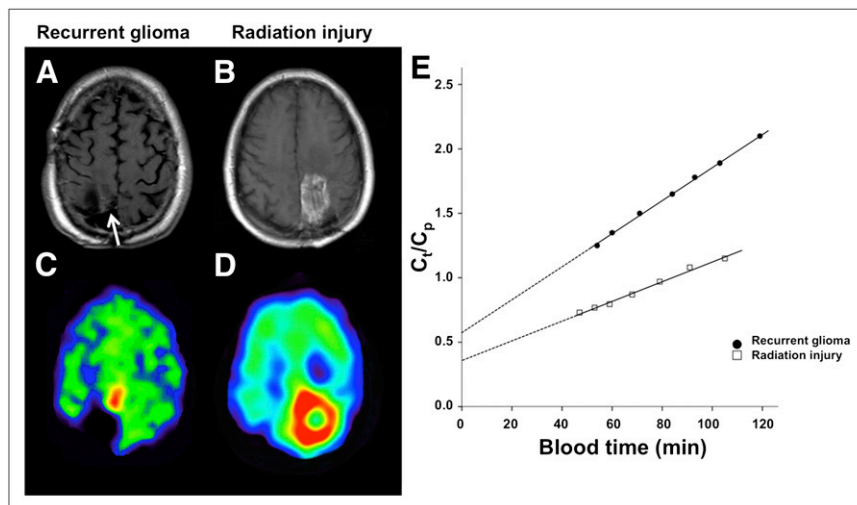
only 0.84 for SUVs and 0.93 for SUV ratios. An SUV ratio cutoff of 1.31 provided 100% sensitivity but only 67% specificity for identifying tumor recurrence; 5 of 10 patients with only radiation injury were falsely classified as having recurrent glioma. VD values and VD ratios provided low differentiating accuracy (AUC, 0.88 and 0.87, respectively). Lesional K-values provided accuracy similar to that of SUV ratio (AUC, 0.91). Finally, in the exploratory analysis of patients with high-grade glioma ($n = 15$), lesion-to-cortex K-ratios provided a complete and robust separation between recurrent tumors ($n = 7$; K-ratio range, 0.94–1.49) and radiation injury ($n = 8$; K-ratio range, 1.70–3.30); any K-ratio cutoff between 1.50 and 1.70 yielded 100% sensitivity and 100% specificity in this patient subgroup.

DISCUSSION

In the present study, we used ^{11}C-AMT PET tracer kinetic analysis of dynamic brain and blood radioactivity data to separate tracer metabolism from transport to distinguish WHO grade II–IV glioma recurrence from radiation injury. Our data show that ^{11}C-AMT SUV in lesions caused by both recurrent tumor and radiation injury is usually higher than that of normal cortex, but the lesion-to-cortex ratio of K, a macroparameter characterizing the unidirectional uptake rate of ^{11}C-AMT, which is related to tryptophan metabolism, provided the most accurate differentiation between recurrent tumors and radiation injury. When the best K-ratio cutoff determined by receiver-operating-characteristic analysis was applied to all patients, there was only 1 false-positive lesion, in a patient whose tumor was originally glioblastoma. When we looked only at those tumors that were originally high-grade, a higher cutoff robustly separated all these tumors from radiation injury. These results suggest that the optimal cutoff may also depend on the original tumor grade.

Radiation-induced brain injury generally appears similar to glioma recurrence as a contrast-enhancing lesion adjacent to the surgical bed on conventional MRI (3). Therefore, standard MRI cannot distinguish reliably between these 2 entities. Among advanced MRI techniques, perfusion MRI and ^{1}H-MRS hold the greatest promise. Regional cerebral blood volume is generally higher in recurrent gliomas than in areas with radiation injury, and this parameter appears to have a high

TABLE 2
Comparison of ^{11}C-AMT PET–Derived Parameters Between Recurrent Tumor and Radiation Injury Groups

^{11}C-AMT PET parameter	All patients			Patients with histology after PET ($n = 13$)		
	Tumor	Radiation injury	P	Tumor	Radiation injury	P
Lesion SUV	2.68 ± 1.05	1.71 ± 0.48	0.014	2.73 ± 1.21	1.97 ± 0.42	0.26
Lesion-to-cortex SUV ratio	2.14 ± 0.68	1.22 ± 0.26	0.001	2.32 ± 0.69	1.45 ± 0.06	0.034
Lesion VD	0.79 ± 0.40	0.41 ± 0.18	0.012	0.82 ± 0.43	0.56 ± 0.19	0.28
Lesion-to-cortex VD ratio	3.33 ± 1.58	1.58 ± 0.66	0.004	3.22 ± 1.39	2.28 ± 0.24	0.21
Lesion K (mL/g/min)	0.012 ± 0.004	0.006 ± 0.002	0.002	0.012 ± 0.005	0.008 ± 0.001	0.10
Lesion-to-cortex K ratio	2.16 ± 0.55	1.18 ± 0.18	0.00003	2.28 ± 0.56	1.29 ± 0.14	0.006

Data are mean ± SD.

differentiating ability (23,24), although it performed relatively poorly in one of the largest series (25). Limitations of perfusion MRI include the potential underestimation of tumor perfusion due to contrast leakage through an impaired blood–brain barrier and low blood flow in low-grade gliomas (4). ^{1}H-MRS is a method capable of characterizing the metabolic properties of a lesion. The feasibility of using multivoxel ^{1}H-MRS techniques in patients with brain tumors has been demonstrated (26), and combined application of diffusion-weighted imaging and ^{1}H-MRS may yield a high diagnostic accuracy in patients treated for high-grade glioma (27). However, ^{1}H-MRS has limited value in detecting small tumors and in evaluating lesions adjacent to scalp, ventricles, calcified structures, surgical clips, and hemorrhage (4). The differentiating ability of ^{18}F-FDG PET has been found to be modest (28,29); this finding is also supported by our observations, although our study was not designed to evaluate the accuracy of ^{18}F-FDG PET.

Amino acid PET tracers accumulate to a greater extent in brain tumor tissue than in normal gray and white matter and are generally superior to standard MRI or ^{18}F-FDG PET in identifying glioma recurrence (5–8,30,31). One posttreatment ^{18}F-FET PET study suggested that analysis of specific time frames of dynamic scans, rather than regular SUVs, may differentiate recurrent gliomas from posttreatment changes with a higher accuracy (10). However, previous posttreatment PET studies did not separate tracer metabolism from transport by quantitative parameters. Our current data show that both transport and, in particular, metabolism of tryptophan is significantly higher in recurrent gliomas than in radiation-related injury, and the sensitivity and specificity of lesion-to-cortex K-ratios is at least comparable to or better than those reported by previous amino acid PET studies. The use of a modified cutoff for tumors that were high-grade on original histology may further improve the differentiating accuracy of this PET parameter. Applying a similar approach might improve differentiation of recurrent gliomas from radiation injury when using other amino acid PET tracers that undergo tumoral metabolism after being transported into the tumor tissue.

Although methionine, tyrosine, and tryptophan use the same transporter to enter into tumor tissue, their metabolic fate is different. The most likely explanation of the high differentiating ability of the ^{11}C-AMT K-ratio is increased metabolism of tryptophan via the kynurenine pathway. As an example of this phenomenon, high concentrations of quinolinic acid, a neurotoxic and epileptogenic metabolite of this pathway, were found in epileptogenic tubers that showed increased ^{11}C-AMT uptake in children with tuberous sclerosis (13,32). Previous studies have also demonstrated that various gliomas, as well as a variety of extracranial tumors, show high expression of indoleamine 2,3-dioxygenase, a key enzyme of the kynurenine pathway (33,34). Indoleamine 2,3-dioxygenase-mediated tryptophan metabolism may lead to proliferation arrest of tumor-invading cytotoxic T lymphocytes because of tryptophan depletion or accumulation of toxic kynurenine metabolites; this is considered to be a major mechanism of compromised antitumoral immune response (33,34).

Although chronic inflammatory processes, leading to increased activity of indoleamine 2,3-dioxygenase, are also involved in the complex pathology of radiation injury (1,35), the kynurenine pathway may not be as markedly upregulated in these lesions as in brain tumors. Postsurgical inflammation can also lead to a transient increase in ^{11}C-AMT uptake at the surgical resection bed, but such effects were not observed beyond 2 mo after resection in patients who had undergone resective epilepsy surgery (36). Nevertheless, prolonged radiation-induced inflammatory changes may lead to increased tryptophan metabolism via the activated kynurenine pathway, thus contributing to unusually high K-values in some patients with radiation injury (such as in patient 14).

The higher transport rate of tryptophan estimated by VD in recurrent gliomas is also not surprising, because the L-type amino acid transporter, which plays a major role in transporting large neutral amino acids through the tumor vascular endothelium, has been shown to be overexpressed in tumor endothelial and glioma cells (37). Methionine uptake by gliomas on PET appeared to correlate with L-type amino acid transporter expression in a recent study (38). Thus, facilitated transport mechanisms, in addition to increased metabolism of tryptophan by glioma cells, may contribute to the good differentiating accuracy of the calculated ^{11}C-AMT kinetic parameters in our study.

This was a study with a relatively small sample size, and a separate evaluation of low-grade tumors was therefore not attempted. The need for venous blood sampling to obtain kinetic ^{11}C-AMT values is somewhat impractical in a clinical setting. Various methods for image-derived input function have been proposed, with mixed success, but new-generation hybrid PET/MRI scanners may help to improve this approach (39). The use of population-derived input function may be another way to possibly eliminate the need for blood sampling (40). Further limitations include the lack of histopathologic verification of tumor recurrence versus radiation injury in about 40% of the patients. However, the differentiating accuracy of lesion-to-cortex K-ratios remained high even when only lesions with histologic verification were included. Our data need to be confirmed by studies in prospective, longitudinal settings and with larger sample sizes. Finally, a direct comparison of ^{11}C-AMT PET with advanced MRI and other PET modalities is necessary to fully evaluate the clinical utility of this technique.

CONCLUSION

Kinetic analysis of dynamic ^{11}C-AMT PET images appears to be highly accurate in differentiating recurrent WHO grade II–IV gliomas from radiation injury. Separation of unidirectional uptake rates from transport can greatly enhance the differentiating accuracy of ^{11}C-AMT PET. This approach may be applied to other amino acid PET tracers that undergo tumoral metabolism, to improve their ability to differentiate recurrent gliomas from radiation injury.

REFERENCES

1. Valk PE, Dillon WP. Radiation injury of the brain. *AJNR.* 1991;12:45–62.
2. Kumar AJ, Leeds NE, Fuller GN, et al. Malignant gliomas: MR imaging spectrum of radiation therapy- and chemotherapy-induced necrosis of the brain after treatment. *Radiology.* 2000;217:377–384.
3. Yang I, Huh NG, Smith ZA, Han SJ, Parsa AT. Distinguishing glioma recurrence from treatment effect after radiochemotherapy and immunotherapy. *Neurosurg Clin N Am.* 2010;21:181–186.
4. Dhermain FG, Hau P, Lanfermann H, Jacobs AH, van den Bent MJ. Advanced MRI and PET imaging for assessment of treatment response in patients with gliomas. *Lancet Neurol.* 2010;9:906–920.
5. Tsuyuguchi N, Takami T, Sunada I, et al. Methionine positron emission tomography for differentiation of recurrent brain tumor and radiation necrosis after stereotactic radiosurgery: in malignant glioma. *Ann Nucl Med.* 2004;18:291–296.
6. Pöpperl G, Götz C, Rachinger W, Gildehaus FJ, Tonn JC, Tatsc K. Value of O-(2-[^{18}F]fluoroethyl)-L-tyrosine PET for the diagnosis of recurrent glioma. *Eur J Nucl Med Mol Imaging.* 2004;31:1464–1470.
7. Rachinger W, Goetz C, Pöpperl G, et al. Positron emission tomography with O-(2-[^{18}F]fluoroethyl)-l-tyrosine versus magnetic resonance imaging in the diagnosis of recurrent gliomas. *Neurosurgery.* 2005;57:505–511.
8. Terakawa Y, Tsuyuguchi N, Iwai Y, et al. Diagnostic accuracy of ^{11}C-methionine PET for differentiation of recurrent brain tumors from radiation necrosis after radiotherapy. *J Nucl Med.* 2008;49:694–699.
9. Grosu AL, Astner ST, Riedel E, et al. An interindividual comparison of O-(2-[^{18}F]fluoroethyl)-L-tyrosine (FET)- and L-[methyl-^{11}C]methionine (MET)-PET in patients with brain gliomas and metastases. *Int J Radiat Oncol Biol Phys.* 2011;81:1049–1058.
10. Pöpperl G, Kreth FW, Herms J, et al. Analysis of ^{18}F-FET PET for grading of recurrent gliomas: is evaluation of uptake kinetics superior to standard methods? *J Nucl Med.* 2006;47:393–403.
11. Madras BK, Sourkes TL. Metabolism of alpha-methyltryptophan. *Biochem Pharmacol.* 1965;14:1499–1506.
12. Diksic M, Nagahiro S, Sourkes TL, Yamamoto YL. A new method to measure brain serotonin synthesis in vivo. I. Theory and basic data for a biological model. *J Cereb Blood Flow Metab.* 1990;10:1–12.
13. Chugani DC, Muzik O. Alpha[C-11]methyl-L-tryptophan PET maps brain serotonin synthesis and kynurenine pathway metabolism. *J Cereb Blood Flow Metab.* 2000;20:2–9.
14. Juhász C, Chugani DC, Muzik O, et al. In vivo uptake and metabolism of alpha-[^{11}C]methyl-L-tryptophan in human brain tumors. *J Cereb Blood Flow Metab.* 2006;26:345–357.
15. Batista CE, Juhász C, Muzik O, et al. Imaging correlates of differential expression of indoleamine 2,3-dioxygenase in human brain tumors. *Mol Imaging Biol.* 2009;11:460–466.
16. Juhász C, Muzik O, Chugani DC, et al. Differential kinetics of alpha-[^{11}C]methyl-L-tryptophan on PET in low-grade brain tumors. *J Neurooncol.* 2011;102:409–415.
17. Suhonen-Polvi H, Ruotsalainen U, Kinnala A, et al. FDG-PET in early infancy: simplified quantification methods to measure cerebral glucose utilization. *J Nucl Med.* 1995;36:1249–1254.
18. Patlak CS, Blasberg RG, Fenstermacher JD. Graphical evaluation of blood-to-brain transfer constants from multiple-time uptake data. *J Cereb Blood Flow Metab.* 1983;3:1–7.
19. Muzik O, Chugani DC, Chakraborty P, Mangner T, Chugani HT. Analysis of [C-11]alpha-methyl-tryptophan kinetics for the estimation of serotonin synthesis rate in vivo. *J Cereb Blood Flow Metab.* 1997;17:659–669.
20. Chugani DC, Muzik O, Chakraborty P, Mangner T, Chugani HT. Human brain serotonin synthesis capacity measured in vivo with alpha-[C-11]methyl-L-tryptophan. *Synapse.* 1998;28:33–43.
21. Diksic M, Leyton M, Benkelfat C. Is alpha-methyl-L-tryptophan a good tracer for brain serotonin synthesis measurements, and does the lumped constant vary in different structures of the rat brain? *J Neurochem.* 1999;73:2621–2624.
22. Gharib A, Balende C, Sarda N, et al. Biochemical and autoradiographic measurements of brain serotonin synthesis rate in the freely moving rat: a reexamination of the alpha-methyl-L-tryptophan method. *J Neurochem.* 1999;72:2593–2600.
23. Hu LS, Baxter LC, Smith KA, et al. Relative cerebral blood volume values to differentiate high-grade glioma recurrence from posttreatment radiation effect: direct correlation between image-guided tissue histopathology and localized dynamic susceptibility-weighted contrast-enhanced perfusion MR imaging measurements. *AJNR.* 2009;30:552–558.
24. Bobek-Billewicz B, Stasik-Pres G, Majchrzak H, Zarudzki L. Differentiation between brain tumor recurrence and radiation injury using perfusion, diffusion-weighted imaging and MR spectroscopy. *Folia Neuropathol.* 2010;48:81–92.
25. Barajas RF Jr, Chang JS, Segal MR, et al. Differentiation of recurrent glioblastoma multiforme from radiation necrosis after external beam radiation therapy with dynamic susceptibility-weighted contrast-enhanced perfusion MR imaging. *Radiology.* 2009;253:486–496.
26. Hollingworth W, Medina LS, Lenkinski RE, et al. A systematic literature review of magnetic resonance spectroscopy for the characterization of brain tumors. *AJNR.* 2006;27:1404–1411.
27. Zeng QS, Li CF, Liu H, Zhen JH, Feng DC. Distinction between recurrent glioma and radiation injury using magnetic resonance spectroscopy in combination with diffusion-weighted imaging. *Int J Radiat Oncol Biol Phys.* 2007;68:151–158.
28. Ricci PE, Karis JP, Heiserman JE, Fram EK, Bice AN, Drayer BP. Differentiating recurrent tumor from radiation necrosis: time for re-evaluation of positron emission tomography? *AJNR.* 1998;19:407–413.
29. Herholz K, Coope D, Jackson A. Metabolic and molecular imaging in neuro-oncology. *Lancet Neurol.* 2007;6:711–724.
30. Chen W, Silverman DH, Delaloye S, et al. ^{18}F-FDOPA PET imaging of brain tumors: comparison study with ^{18}F-FDG PET and evaluation of diagnostic accuracy. *J Nucl Med.* 2006;47:904–911.
31. Mehrkens JH, Popperl G, Rachinger W, et al. The positive predictive value of O-(2-[^{18}F]fluoroethyl)-L-tyrosine (FET) PET in the diagnosis of a glioma recurrence after multimodal treatment. *J Neurooncol.* 2008;88:27–35.
32. Chugani DC, Chugani HT, Muzik O, et al. Imaging epileptogenic tubers in children with tuberous sclerosis complex using alpha-[^{11}C]methyl-L-tryptophan positron emission tomography. *Ann Neurol.* 1998;44:858–866.
33. Uyttenhove C, Pilotte L, Theate I, et al. Evidence for a tumoral immune resistance mechanism based on tryptophan degradation by indoleamine 2,3-dioxygenase. *Nat Med.* 2003;9:1269–1274.
34. Munn DH, Mellor AL. Indoleamine 2,3-dioxygenase and tumor-induced tolerance. *J Clin Invest.* 2007;117:1147–1154.
35. Yoshii Y. Pathological review of late cerebral radionecrosis. *Brain Tumor Pathol.* 2008;25:51–58.
36. Juhász C, Chugani DC, Padhye UN, et al. Evaluation with alpha-[^{11}C]methyl-L-tryptophan positron emission tomography for reoperation after failed epilepsy surgery. *Epilepsia.* 2004;45:124–130.
37. Kobayashi K, Ohnishi A, Promsuk J, et al. Enhanced tumor growth elicited by L-type amino acid transporter 1 in human malignant glioma cells. *Neurosurgery.* 2008;62:493–503.
38. Okubo S, Zhen HN, Kawai N, Nishiyama Y, Haba R, Tamiya T. Correlation of L-methyl-^{11}C-methionine (MET) uptake with L-type amino acid transporter 1 in human gliomas. *J Neurooncol.* 2010;99:217–225.
39. Zanotti-Fregonara P, Chen K, Liow JS, Fujita M, Innis RB. Image-derived input function for brain PET studies: many challenges and few opportunities. *J Cereb Blood Flow Metab.* 2011;31:1986–1998.
40. Eberl S, Anayat AR, Fulton RR, Hooper PK, Fulham MJ. Evaluation of two population-based input functions for quantitative neurological FDG PET studies. *Eur J Nucl Med.* 1997;24:299–304.